ADSORPTIVE AND PHOTOCATALYTIC PROPERTIES OF THE ZnO/BENTONITE/Ag HETEROJUNCTION

Oleksiy Klimenkov[1], *Iryna Ivanenko*[1]

[1]National Technical University of Ukraine "Igor Sikorsky Kyiv Polytechnic Institute",

Beresteisky Avenue, 37, Kyiv, 03056, Ukraine, aleshaklemenkov@gmail.com

DOI: https://doi.org/10.20535/2218-930032023301934

The degradation of organic wastewater pollutants from diverse sources represents a critical scientific challenge, particularly in light of the escalating demand for dyes across various industries. Addressing this challenge entails the exploration of efficient and eco-friendly methods to convert organic pollutants into benign and straightforward compounds, leveraging state-of-the-art photocatalysts. The synthesis was conducted via the novel sol-gel method. Structural, crystalline, elemental and phase parameters were analyzed using X-ray analysis, chemical surface characteristics investigated through infrared spectroscopy, band gap determination performed via diffuse reflectance spectroscopy, and evaluation of adsorption and photocatalytic activity carried out for the semiconductor photocatalyst ZnO and heterojunctions incorporating bentonite. The synthesized photocatalysts were employed for the removal of malachite green dye. Equilibrium studies for adsorption were conducted using Langmuir and Freundlich isotherms, revealing a superior fit with the Langmuir model. The maximum adsorption capacity was determined as 70.4 mg/g using the Langmuir equation. Kinetic parameters indicated that the adsorption of malachite green on bentonite followed a first-order kinetics model where k_1=0,152 min^{-1}. The photodegradation efficiency of ZnO, ZnO/bentonite, and Zn/bentonite/Ag was investigated by static experiment under ultraviolet irradiation. Within 60 minutes, a 99.4% photodegradation of the malachite green solution at a concentration of 100 mg/L was achieved using the ternary heterojunction photocatalyst. Remarkably, within just 10 minutes in the presence of the ternary composite, a degree of photocatalytic degradation reaching 72% was attained, which significantly exceeds the results of the binary heterojunction photocatalyst. Thus, the synthesized heterojunction exhibits notable photocatalytic activity, particularly evident within short time intervals. A proposed mechanism for the photocatalytic degradation of malachite green is outlined based on existing literature sources.

Key words: *bentonite, heterojunction, malachite green, photocatalyst, sol-gel, zinc oxide*

Received: 20 December 2023 Revised: 3 January 2024 Accepted: 4 January 2024

1. Introduction

Today, the issue of wastewater pollution with dyes has escalated to a global scale, primarily due to the rapid expansion of industries such as paper, textile, dye, food, and pharmaceuticals. This expansion is attributed to industrialization and population growth, exacerbating the environmental challenges associated with dye effluents (Khan et al., 2023). Annually, more than 200,000 tons of wastewater, containing high concentrations of various types of dyes, are discharged untreated into water bodies by industrial enterprises (Anantha et al., 2020). Dyes are notorious for their unpredictable impact on living organisms, often leading to chronic diseases and intoxication upon prolonged exposure. Due to their varied chemical interactions, degrading dyes into simple and harmless compounds is challenging, particularly in real wastewater scenarios. Despite these challenges, advancements in physical and chemical

techniques such as precipitation, coagulation, adsorption, flocculation, oxidation, and electrocoagulation continue to progress rapidly. However, leading methods in wastewater treatment encompass adsorption, photocatalysis, reactive oxidation, and membrane separation.

Photocatalysis, in particular, stands out among modern oxidative techniques due to its affordability, rapidity, and non-selectivity for organic pollutants. Semiconductors or their composites serve as photoactive agents, with the capability to form heterojunctions.

Wurtzite Zinc Oxide (ZnO) is an n-type semiconductor and a well-established standard photocatalyst utilized in water treatment processes aimed at mitigating hazardous and persistent organic and inorganic pollutants. It facilitates their conversion into low molecular weight molecules, water, carbon dioxide, and non-toxic inorganic mineral ions (Freitas et al., 2022).

ZnO is a highly promising photocatalyst owing to its distinctive crystalline structure, exceptional photosensitivity, elevated electron mobility, non-toxic nature, and cost-effectiveness (Bogatu et al., 2023). Other notable properties of ZnO include its wide band gap (3.37 eV) in the near-UV spectrum, robust oxidizing capabilities, high excitation binding energy (60 meV), and its ability to generate electron-hole pairs under UV and visible light irradiation (Chen et al., 2017). The exploration and advancement of various systems utilizing clay minerals as fundamental constituents are noteworthy due to their environmentally friendly characteristics, ample global reservoirs, cost-effectiveness, and high applicability across industries. Bentonite, in particular, exhibits remarkable technological suitability attributed to its exceptional adsorption capacity, barrier properties, cation exchange capacity, and substantial swelling capacity (Pourhakkak et al., 2021). Many recent studies show the modification and further application of bentonite in heterogeneous photocatalysis for the degradation of textile dyes (Javanbakht and Mohammadian 2021). Silver (Ag)-based semiconductor materials have garnered significant interest owing to their narrow bandgap and outstanding photocatalytic efficacy within the visible light spectrum. Silver possesses a narrow band gap (ranging from 2.08 to 2.46 eV), enabling it to absorb a broad spectrum of visible light. Additionally, hybridization with Ag^+ can mitigate the reactivity of conduction band electrons while facilitating the separation of photogenerated electron-hole pairs, thereby enhancing its photocatalytic performance (Bian et al., 2020).

However, the widespread implementation of heterojunctions is currently limited by their relatively low photocatalytic activity and stability. These two parameters directly depend on the ability to absorb enough light, electron-hole pair activation/recombination, etc. Addressing these challenges often involves optimizing the band gap of the heterojunction, which serves as a partial solution to enhance their performance (Zhang et al., 2018). Although, non-trivial challenges impede progress: when incorporating other transition metal compounds into semiconductors, achieving uniform loading on the photocatalyst presents a significant obstacle. Consequently, striking a compromise between maintaining high catalytic activity and attaining desired physical and chemical properties becomes complex (Murakami et al., 2010). Also, the photocatalytic mechanism and structural

activity of heterojunctions are not fully understood due to the unpredictability of the most energetically advantageous paths of degradation reactions and the formation of their intermediate compounds (Chen et al., 2021). The aim of the presented work was to prove that the formation of a ZnO heterojunction with a bentonite matrix has a positive effect on the kinetics and equilibrium of adsorption and photocatalytic processes, while Argentum doping eliminates the recombination effect. For this, the following tasks were solved: to synthesize double and triple heterojunctions of zinc oxide; to study the phase composition and structural-crystalline parameters of pure ZnO and both of its heterojunctions, as well as to investigate and compare their photocatalytic activity.

2. Materials and methods

The following reagents were used for the synthesis and research of samples of heterojunction photocatalysts: pure anhydrous zinc acetate ($Zn(CH_3COO)_2$ (Ukraine)), ethanol (C_2H_5OH 96% (Ukraine)), sodium hydroxide (NaOH (Ukraine)), argentum nitrate ($AgNO_3$ (Ukraine)), bentonite (bentonite clay (Ukraine)), malachite green (dye $C_{23}H_{25}ClN_2$ (Ukraine)).

2.1 Synthesis

The pure ZnO sample was obtained as discribed in (Klimenkov et al., 2023).

The synthesis of the heterojunction was conducted via the sol-gel method. Initially, solutions of zinc acetate and silver nitrate in ethanol, with concentrations of 0.18 mol/L and 0.012 mol/L respectively, were prepared by dissolving for 10 hours at a temperature of 80°C. Subsequently, the mixture was cooled to 0°C using an ice bath, and dropwise addition of an aqueous solution of NaOH with a concentration of 0.44 mol/L ensued, resulting in hydrolysis and the formation of a gray gel. Bentonite, pre-fired at 400°C, was combined with the filtered gel post-hydrolysis. The gel underwent an aging stage for three days, followed by drying for 1 hour at 100°C, and ultimately calcination for three hours at 500°C, yielding the synthesis product is an yellow ZnO/bentonite/Ag powder.

2.2 Instrumental methods

X-ray phase analysis was conducted using a Rigaku Ultima IV diffractometer (Japan) equipped with CuKα radiation. The samples were subjected to examination under copper radiation (CuKα = 0.15418 nm, 40 kW, 30 mA). IR analysis was carried out using the IRXross Fourier Transform Infrared (FTIR) Spectrophotometer. Diffuse Reflectance Spectroscopy and UV-Vis analysis were performed utilizing a UV-Vis spectrophotometer UV-2600i.

The band gap width was determined using the Kubelka-Munk method according to the following procedure. Reflectance values (R) obtained were converted into dimensionless values by dividing by 100:

$$R = \frac{R\%}{100}.$$

The absorption coefficient (k, m^{-1}) was calculated using the following formula:

$$k = (1 - R)^2.$$

The scattering coefficient (s, m^{-1}) was calculated according to the formula:

$$s = 2R.$$

Both calculated values were substituted into the Kubelka-Munk formula:

$$F(R) = \frac{k}{s}.$$

Wavelength values were converted into photon energy (E, eV) according to Einstein's formula:

$$E = \frac{hc}{\lambda},$$

where h is Planck's constant, 6.63×10^{-34} J×s; c is the speed of light, 3.00×10^{8} m/s; λ is the wavelength, cm^{-1}.

The dependencies $[F(R)E]^{1/2}=f(E)$ and $[F(R)E]^{2}=f(E)$ were established The dependency with the highest correlation was determined using graphical methods. The optical band gap value was derived by identifying the tangent that intersects the largest segment on its abscissa axis (refer to Figures 3 and 4) (Philips-Invernizzi, Dupont and Caze 2001).

2.3 Adsorptive and photocatalytic experiments

To evaluate the photocatalytic activity of the synthesized samples, static tests were conducted. An Osram Puritec HNS G5 8W G8T5 UV lamp with a wavelength of 288 nm (China) was employed for this purpose. A solution of malachite green with a concentration of 100 mg/L was prepared. 15 ml of the dye solution was then transferred to a beaker and subjected to UV irradiation for 2, 5, 10, 30, and 60 minutes. Subsequently, the sediment was filtered using a syringe with a membrane nozzle, and the solution was analyzed using a UV-Vis spectrophotometer. The adsorption properties of bentonite were evaluated under the same conditions but without UV irradiation in the dark. The dye photodegradation and the adsorption efficiency of bentonite were calculated using the following formulas:

$$\%\ Dye\ photodegradation = \frac{C_0 - C_t}{C_0} \cdot 100;$$

$$\%\ Adsorbtion\ efficiency = \frac{C_0 - C_t}{C_0} \cdot 100.$$

2.4 Adsorption isotherm

Adsorption isotherms provide valuable insights into the mechanism of adsorbate distribution between the solid and liquid phases at equilibrium (Zhuang et al., 2016). The Langmuir and Freundlich equations were used to calculate malachite green dye adsorption isotherms in bentonite pores. The Langmuir equation is used to describe monolayer chemisorption processes, while the Freundlich equation is useful for studying multilayer systems. The Langmuir isotherm model is described by the equation:

$$Q_e = \frac{bC_e}{1+bC_e},$$

where Q_e – equilibrium adsorption capacity, mg/g; C_e – equilibrium concentration of the adsorbate, mg/L; $b = \frac{k_1}{k_2}$ – adsorption coefficient, which is determined by the ratio of equilibrium constants that depend on temperature and determine the shape of the adsorption isotherm.

The dimensionless separation factor R_L was calculated by the formula:

$$R_L = \frac{1}{1 + bC_e}.$$

Adsorption is unacceptable if $R_L > 1$, linear if $R_L = 1$, desirable if $0 < R_L < 1$, irreversible if $R_L=0$. The Freundlich model is described by the following equation:

$$lnQ_e = \frac{1}{n_F} lnC_e + lnK_F,$$

where n_F and K_F – Freundlich constants.

2.5 Adsorption kinetics

The kinetic models for malachite green adsorption on the bentonite surface were determined using the first-order and pseudo-second-order Lagergren equations (Liang et al., 2010).

The first-order kinetic equation was linearized to graphically ascertain the rate constant:

$$\ln(Q_e - Q_t) = lnQ_e - \frac{k_1}{2.303}\tau,$$

where Q_e – amount of adsorbed dye, mg/g; Q_t - equilibrium amount of adsorbed dye over

time τ, mg/g; k_1 – pseudo-first order rate constant, min^{-1}. (Elkady, Mahmoud and Abd-El-Rahman 2011).The equation of the pseudo-second kinetic model can be expressed as:

$$\frac{Q_e}{Q_t(Q_t - Q_e)} = k_2\tau,$$

where k_2 – second-order rate constant.

3. Results and discussions

3.1 Characterisation of pure ZnO and its heterojunctions

The diffraction pattern of pure ZnO in Figure 1-a reveals a remarkably clean hexagonal (wurtzite) structure with characteristic diffraction peaks at 2-θ = 32°, 34°, 36°, 48°, 57°, 63°, 66°, 68°, and 69°. This confirms the 100% degree of crystallinity of the zinc oxide, underscoring the efficacy of the chosen synthesis method. The crystallite size, computed using the Williamson-Hall method, was determined to be 34.8 nm, validating the nanodispersity of the synthesized pure ZnO powder.

X-ray phase analysis of the ZnO/bentonite and ZnO/bentonite/Ag heterojunctions revealed the mainly presence of quartz SiO_2 and aluminum oxide Al_2O_3 in their composition (Figure 1-b and 1-c). The characteristic diffraction peaks of SiO_2 are located at positions 20°, 27°, 60°, and 61.5°, while those of Al_2O_3 appear at 32°, 47.8°, and 50°. A triplet at 2θ = 34.8°, 35.5°, 36.5°, as well as the peak at 2θ = 68°, indicate the presence of the wurtzite structure of ZnO. The diffraction peak at 2θ = 56.8° suggests the presence of doped silver. The crystallite sizes of ZnO/bentonite and ZnO/bentonite/Ag were determined to be 5.0 nm and 4.7 nm, respectively. Analysis of the obtained data suggests that the ZnO phase is incorporated and evenly distributed within the monolayer or submonolayer structure of the bentonite matrix, while maintaining its crystalline structure (Ahmad et al., 2019).

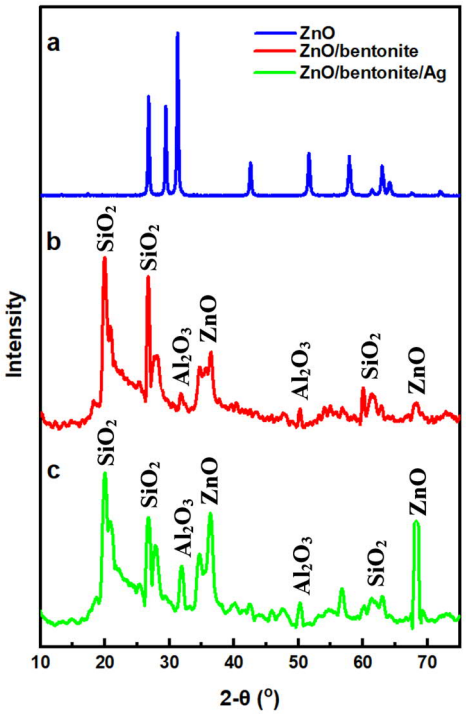

Fig. 1. *Diffraction patterns of pure ZnO, ZnO/bentonite and ZnO/bentonite/Ag heterojunctions*

The surface chemistry of the synthesized samples was investigated using the infrared spectroscopy method. In the IR spectrum of pure ZnO (Figure 2-a), a single prominent peak is observed at 419 cm^{-1}, corresponding to the vibrations of the Zn=O bond (Zhuang et al., 2022).

The IR spectra of ZnO/bentonite and ZnO/bentonite/Ag heterojunctions (Figures 2-b and 2-c) exhibit a characteristic peak of ZnO at a wavelength of 419 cm^{-1}. Additionally, multiple bands observed at 3672 cm^{-1} correspond to the Al-OH-Al bond in bentonite (Gupta 2013). The two sharp bands observed at 2988 and 2901 cm^{-1} are attributed to overtones and combination tones in SiO_4 silicate. The sharp and intense band at 1395 cm^{-1} appears from the asymmetric stretching of OH (deformation mode) of water, which is also a structural component of the mineral. The sharp component of the maximum absorption band at 1020 cm^{-1} is characteristic of the layered silicate mineral montmorillonite and is attributed to the triply degenerate stretching vibration of Si-O. The band observed at 799 cm^{-1} is associated with the deformation type Al-Al-OH or Al-OH-Al (Philips-Invernizzi, Dupont and Caze 2001). The mass concentration of silver in the heterojunction reaches 1 wt%, which proved to be insufficient for its identification on the IR spectrum. Therefore, X-ray diffraction is more suitable for identifying silver in this sample.

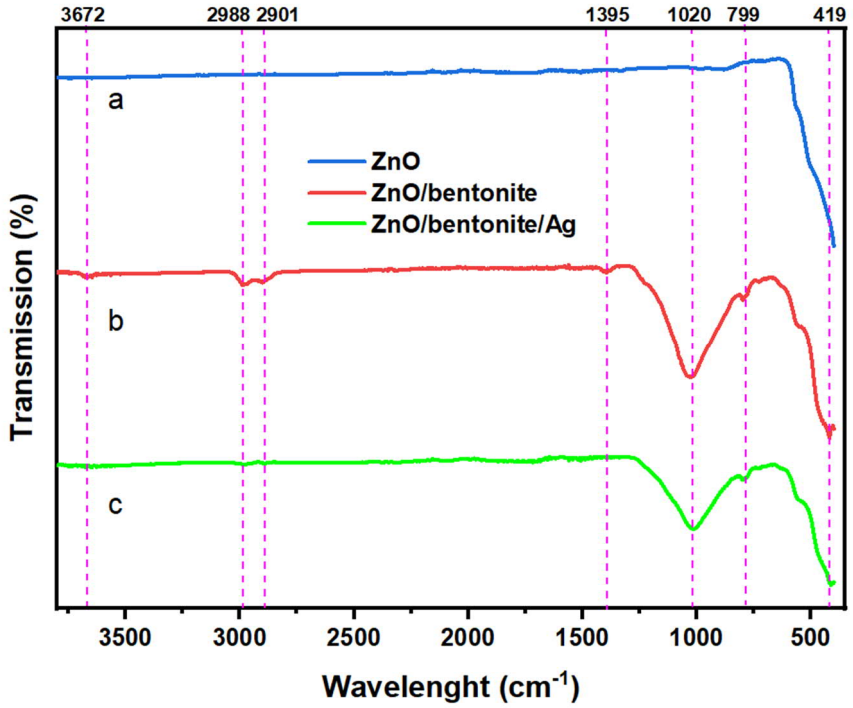

Fig. 2. *IR spectra of pure Zn, ZnO/bentonite and ZnO/bentonite/Ag heterojunctions*

The diffuse reflectance spectra of the synthesized samples (Figure 3) were obtained to determine their optical band gap, which was calculated using the Kubelka-Munk method (Figure 4).

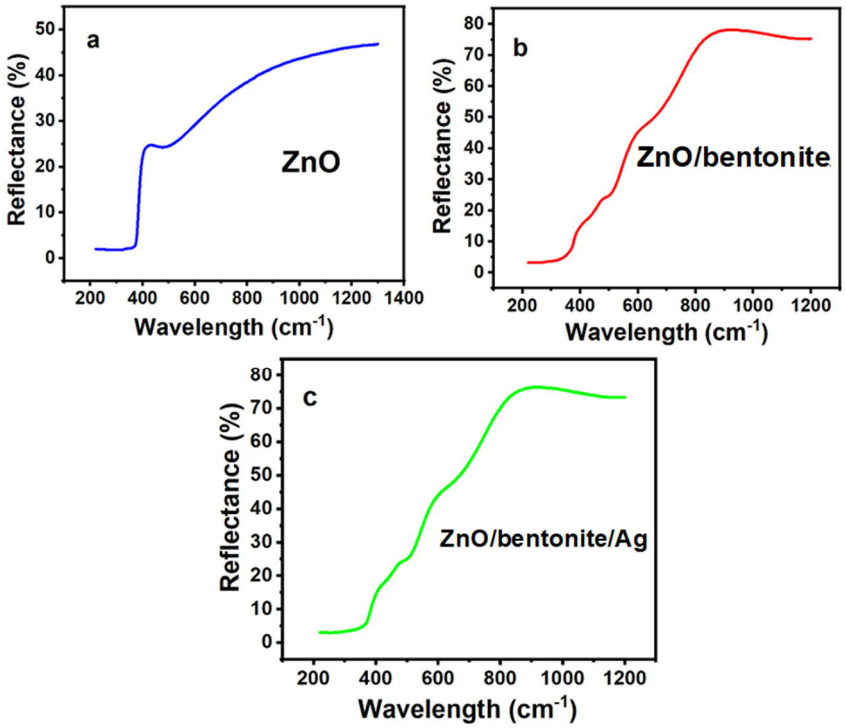

Fig. 3. *Diffusion reflection spectra of pure ZnO, ZnO/bentonite and ZnO/bentonite/Ag heterojunctions*

The synthesized ZnO/bentonite/Ag heterojunction exhibits a smaller optical bandgap wich equvals 2.9 eV. The ZnO/bentonite heterojunction has optical bandgap in 0.03 eV biger. The optical bandgap of pure ZnO semiconductor photocatalyst constituted 3.13 eV, and was the widest.

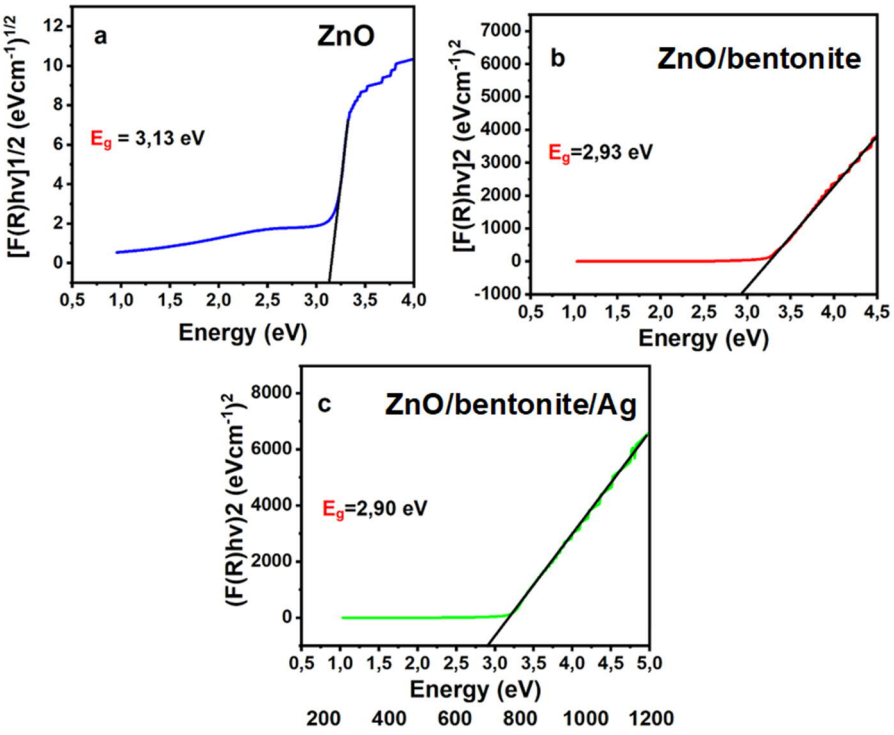

Fig. 4. *Optical band gap of pure ZnO, ZnO/bentonite and ZnO/bentonite/Ag heterojunctions*

It is known, that reducing the band gap weakens the recombination effect, thereby exerting a positive influence on the photocatalytic activity of the heterojunction. That is why the next stage of the current research was to study the activity of the synthesized samples in a model photocatalytic reaction.

3.2 Adsorption properties of the initial bentonite

Photocatalytic tests were began with studying the adsorption characteristics of the original bentonite, based on the following considerations: the initial stage of any heterogeneous photocatalytic process is adsorption absorption; Bentonite clay has high porosity and a developed internal surface, so the share of adsorption in the overall process cannot be excluded.

The adsorbtion isotherm of malachite green (MG) on the surface of bentonite (Figure 5) has a form characteristic of the Langmuir adsorption isotherm. Bentonite demonstrated a notably high adsorption capacity, with 80% of the MG being adsorbed within 30 minutes. The maximum adsorption of 96% was attained within 50-60 minutes, and the isotherm reaches a horizontal plateau.

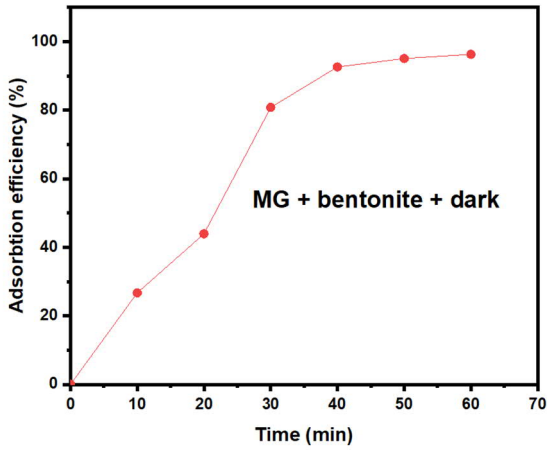

Fig. 5. *Adsorption isotherm of malachite green on bentonite*

The relationship between the adsorption of MG dye on the bentonite surface with the Langmuir and Freundlich isotherms was investigated, and the results are presented in Table 1. The data for MG removal were fitted by the Langmuir isotherm and compared to the Freundlich isotherm.

Table 1. *Langmuir and Freundlich parameters for MG adsorption*

Langmuir model			**Freundlich model**			$\mathbf{R_L}$
$\mathbf{Q_0}$, **mg/g**	**b**	$\mathbf{R^2}$	$\mathbf{K_F}$, **mg/g**	$\mathbf{n_F}$	$\mathbf{R^2}$	0.03
70.4	0.295	0.924	9.41	2.581	0.846	

The adsorption capacity of MG according to Langmuir and Freundlich was equal to 70.44 and 9.41 mg/g, respectively. The values of Langmuir partition coefficient R_L were in the range of 0-1, which is evidence that the adsorption process was possible, and

the value of R_L (<0.1) proves the effective interaction between the dye and the adsorbent (Olivera et al., 2018).

Kinetic models are developed to comprehend the reaction rate of the adsorption process. The stages of MG removal using bentonite were analyzed using first-order and pseudo-second-order Lagergren kinetic models. From Table 2, it can be observed that the squared values of the regressioncorrelation coefficient (R^2) of the rate of the first-order Lagergren kinetic model were sufficiently high.

Table 2. *First- and pseudo-second-order kinetic parameters of MG adsorption*

First-order kinetic model			**Pseudo-second order kinetic model**		
Q_e, mg/g	**k_1 min^{-1}**	**R^2**	**Q_e, mg/g**	**k_2 min^{-1}**	**R^2**
45.05	0.152	0.957	54.96	0.0182	0.944

A pseudo-second-order kinetic model elucidates the rate mechanism of the reaction by chemisorption. The graph of the pseudo-second-order kinetic model is depicted in Figure 6-A.

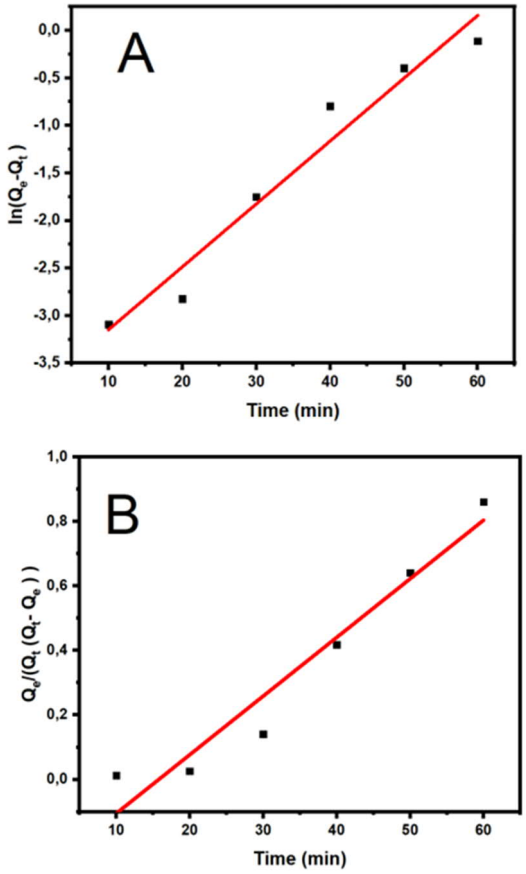

Fig. 6. *Kinetic model of the first-order(A) and pseudo-second-order (B) adsorption*

In Figure 6-B, the graph does not pass through the origin, indicating that the speed of the adsorption process depends on various kinetic factors, as well as diffusion within the particles.

3.3 Photocatalytic tests

The dependence of the degree of photodegradation of the malachite green dye over time (Figure 7) demonstrates that MG decomposes by 21.4 % in an hour under the influence of ultraviolet radiation even without a photocatalyst, however, in the presence of ZnO/bentonite/Ag heterojunction, almost complete decomposition was achieved over the same period of time.

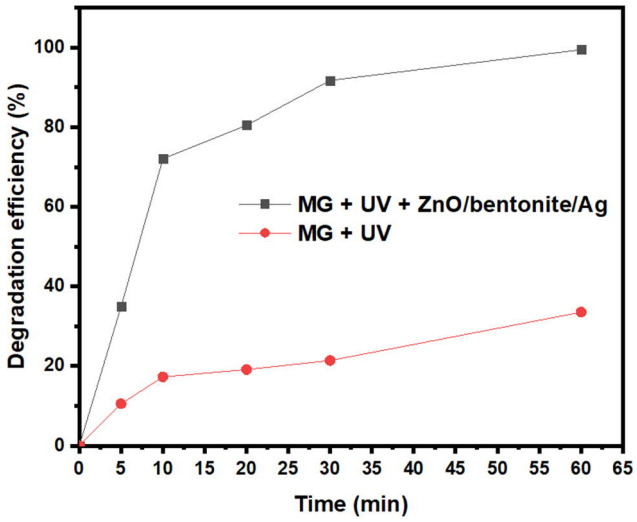

Fig. 7*. MG photodegradation without photocatalyst and in the presence of ZnO/bentonite/Ag heterojunction*

In the initial 30 minutes, a 92% photocatalytic degradation was achieved, and after 60 minutes, the degree of MG degradation of 99.4% was attained. The self-degradation of the MG solution under UV irradiation did not exceed 21.4% in 30 minutes.

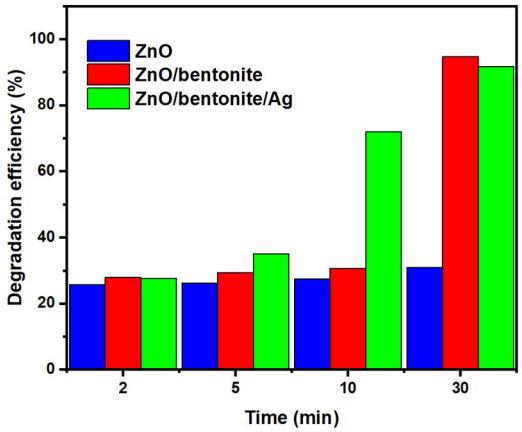

Fig. 8. *Degree of photocatalytic degradation of MG in the presence of ZnO, ZnO/bentonite and ZnO/bentonite/Ag heterojunctions*

The histogram (Figure 8) allows to evaluate the degree of photocatalytic decomposition of MG in the presence of pure ZnO, ZnO/bentonite and ZnO/bentonite/Ag heterojunctions and compare their photocatalytic activity.

In the presence of the synthesized ZnO/bentonite and ZnO/bentonite/Ag heterojunctions, nearly 95% and 92% degradation of the studied dye was achieved within half an hour of UV irradiation, respectively. Moreover, within 10 minutes in the presence of the ternary composite, the degree of photocatalytic degradation reached 72%, nearly 2.5 times more of magnitude higher than that of the double heterojunction. Consequently, the both synthesized heterojunctions exhibit high photocatalytic activity, but for a triple ZnO/bentonite/Ag heterojunction it particularly evident within short time intervals.

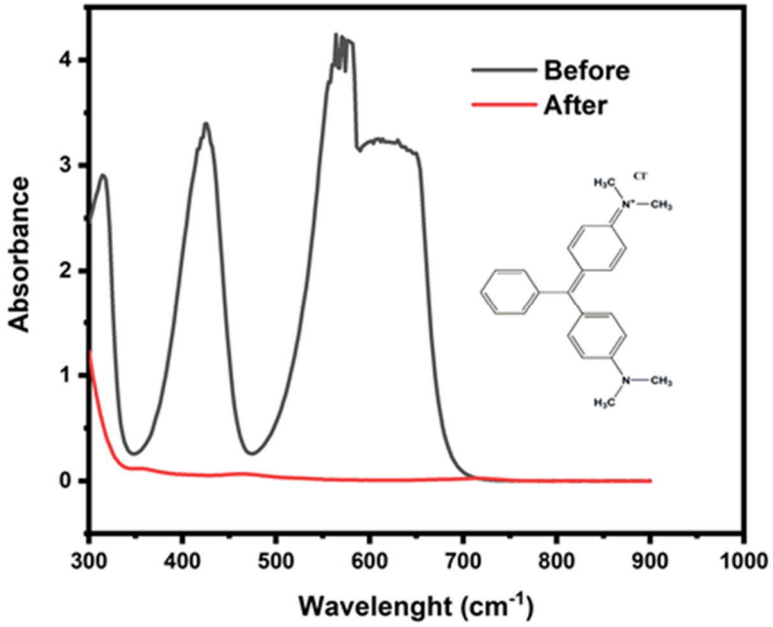

Fig. 9. *UV spectrum of MG before and after photocatalytic experiment*

The UV spectrum of malachite green (100 mg/L) in the Figure 9 demonstrates and proves complete photodecomposition of the studied dye under the influence of ultraviolet radiation in the presence of a triple ZnO/bentonite/Ag heterojunction.

3.4 Possible mechanism of photocatalytic degradation

MG initially adsorbs onto the surface of the catalyst and absorbs UV light, thus enhancing photocatalysis. Through the excited state, it introduces an electron into the conduction band of the catalyst. This electron can subsequently react with adsorbed oxygen and water, leading to the formation of a superoxide radical and ultimately a hydroxyl radical, both of which are responsible for the degradation of MG. The complex absorption properties of the catalyst in the near-ultraviolet light region contribute to the higher photocatalytic degradation of MG. The process of MG bond breaking and the formation of intermediate compounds is illustrated in Figure 10 (Amigun et al., 2022).

These intermediates are ultimately converted to non-toxic products such as CO_2 and H_2O by reactive superoxide and hydroxyl radicals.

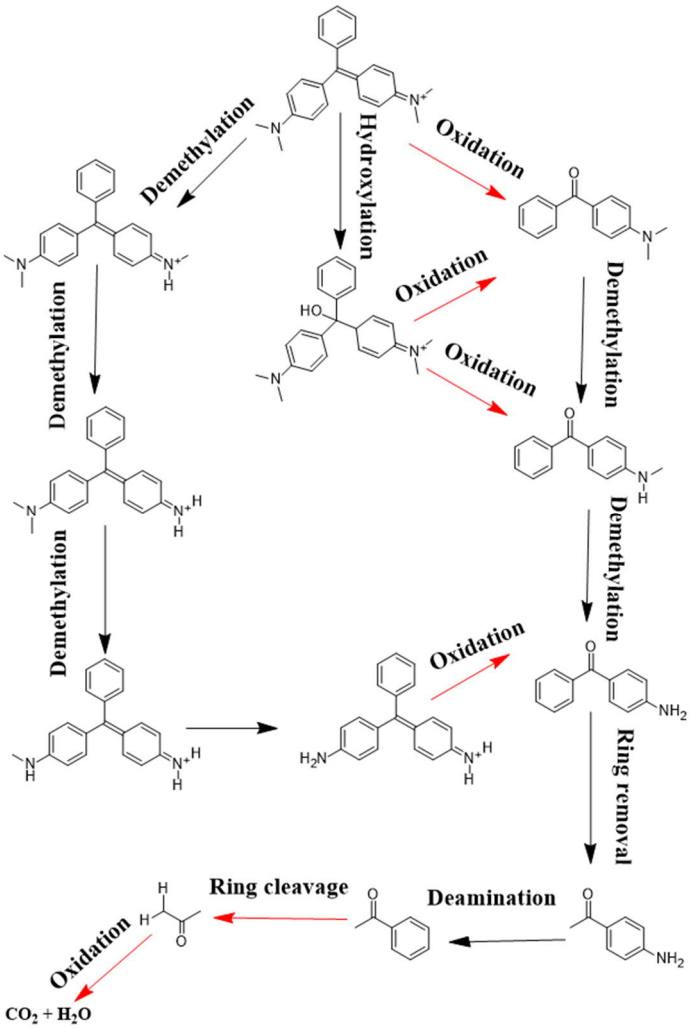

Fig. 10. *Path of MG degradation (Amigun, Adekola, Tijani and Mustapha 2022)*

The mechanism of the photocatalytic process can be expressed as follows:

$$Catalyst + hv \rightarrow Catalyst^{+} + e^{-}$$

$$e^{-} + O_2 \rightarrow O^{\bullet 2-}$$

$$Catalyst^{+} \rightarrow Catalyst + h^{+}$$

$$h^{+} + H_2O/OH^{-} \rightarrow HO^{\bullet}$$

$$MG + HO^{\bullet} / O_2^{\bullet -} \rightarrow CO_2 + H_2O$$

During the photocatalytic degradation of MG, several chemical transformations occur, including hydroxylation, demethylation, oxidation, deamination, and benzene ring cleavage. Further degradation progresses towards complete mineralization (Barapatre, Aadil and Jha 2017).

4. Conclusions

Samples of pure zinc oxide and its heterojunctions, based on pure bentonite and doped with silver, were synthesized using an

innovative sol-gel method without the need for expensive or toxic reagents.

X-ray diffraction analysis revealed the presence of a pure hexagonal (wurtzite) ZnO structure in all synthesized samples. Additionally, X-ray structural analysis identified smaller crystallites (5.0 and 4.7 nm) in the ZnO/bentonite and ZnO/bentonite/Ag heterojunctions, respectively.

The surface chemistry of the synthesized samples of ZnO, ZnO/bentonite, and ZnO/bentonite/Ag was examined using IR spectroscopy, confirming the presence of a characteristic band for the Zn=O bond (419 cm^{-1}) in all spectra. Furthermore, the main component of the bentonite structure, montmorillonite, exhibited a characteristic band at 1020 cm^{-1}.

Experimental evidence confirmed that the ZnO/bentonite/Ag heterojunction possesses a smaller band gap compared to pure ZnO and ZnO/bentonite (2.90, 2.93, and 3.13 eV, respectively). This reduction in band gap makes the electron-hole pair formation process less energy-intensive, thereby enhancing the photocatalytic activity.

The highest photocatalytic degradation (99.4% in 60 min) was achieved using the triple heterojunction ZnO/bentonite/Ag.

Langmuir and Freundlich adsorption isotherms were calculated, with the partition coefficient RL found to be less than unity, indicating effective interaction between the dye and the adsorbent.

The adsorption rate of bentonite was estimated using first and pseudo-second-order kinetic models, with calculated rate constants ($k_1 = 0.152$, $k_2 = 0.0182$).

Based on literature sources analysis, a mechanism of photocatalytic degradation of malachite green using the ZnO/bentonite/Ag heterojunction was proposed.

References

1. Ahmad, S.; Su, X.; Yang, C.; Wang, X.; Liu, X.; Wang, J. Space-confined growth of layered basic zinc acetate nanosheets and their orderly fragmented ZnO nanoparticles on clay platelets. *J. Hazard. Mater.* **2019**, *371*, 213–223. https://doi.org/10.1016/j.jhazmat.2019.02.111.

2. Amigun, A. T.; Adekola, F. A.; Tijani, J. O.; Mustapha, S. Photocatalytic degradation of malachite green dye using nitrogen/sodium/iron-TiO_2 nanocatalysts. *Results Chem.* **2022**, *4*, 100480. https://doi.org/10.1016/j.rechem.2022.100480.

3. Anantha, M. S.; Olivera, S.; Hu, C.; Jayanna, B. K.; Reddy, N.; Venkatesh, K.; Muralidhara, H. B.; Naidu, R. Comparison of the photocatalytic, adsorption and electrochemical methods for the removal of cationic dyes from aqueous solutions. *Environ Technol Inno.* **2020**, *17*, 100612. https://doi.org/10.1016/j.eti.2020.100612.

4. Barapatre, A.; Aadil, K. R.; Jha, H. Biodegradation of Malachite Green by the Ligninolytic Fungus Aspergillus flavus. *CLEAN – Soil, Air, Water* 2017, 45 (4), 1600045. https://doi.org/10.1002/clen.201600045.

5. Bian, H.; Zhang, Z.; Xu, X.; Gao, Y.; Wang, T. Photocatalytic activity of Ag/ZnO /AgO/TiO_2 composite. *Phys. E: Low-Dimens. Syst. Nanostructures*. **2020**, *124*, 114236. https://doi.org/10.1016/j.physe.2020.114236.

6. Bogatu, C.; Covei, M.; Polo-López, M. I.; Duta, A.; Malato, S. Novel ZnO photocatalysts for pollutants' abatement under solar radiation at pilot plant scale. *Catal. Today* **2023**, *413-415*, 113947. https://doi.org/10.1016/j.cattod.2022.11.008.

7. Chen, X.; Liu, A.; Chen, Q.; Liu, Y.; Zou, L.; McKeown, M. J. Simultaneous ocular and muscle artifact removal from EEG data by exploiting diverse statistics. *Comput Biol Med* **2017**, *88*, 1–10. https://doi.org/10.1016/j.compbiomed.2017.06.013.

8. Chen, Y.; Xu, M.; Wen, J.; Wan, Y.; Zhao, Q.; Cao, X.; Ding, Y.; Wang, Z. L.; Li, H.; Bian, Z. Selective recovery of precious metals through photocatalysis. *Nat. Sustain.* **2021**, *4* (7), 618–626. https://doi.org/10.1038/s41893-021-00697-4.

9. Elkady, M. F.; Mahmoud, M. M.; Abd-El-Rahman, H. M. Kinetic approach for cadmium sorption using microwave synthesized nano-hydroxyapatite. *Journal of Non-Crystalline Solids* **2011**, *357* (3), 1118–1129. https://doi.org/10.1016/j.jnoncrysol.2010.10.021.

10. Freitas, W. A.; Soares, B. E. C. F.; Rodrigues, M. S.; Trigueiro, P.; Honorio, L. M. C.; Peña-Garcia, R.; Alcântara, A. C. S.; Silva-Filho, E. C.; Fonseca, M. G.; Furtini, M. B.; et al. Facile synthesis of ZnO-clay minerals composites using an ultrasonic approach for photocatalytic performance. *J. Photochem. Photobiol. A: Chem.* **2022**, *429*, 113934. https://doi.org/10.1016/j.jphotochem.2022.113934.

11. Gupta, A. K. XRF Studies for Chemical Composition and Molecular Formula of Jharkhand Bentonite. *OSR-JAC* **2013**, *4*, 42–46.

12. Javanbakht, V.; Mohammadian, M. Photo-assisted advanced oxidation processes for efficient removal of anionic and cationic dyes using Bentonite/TiO_2 nano-photocatalyst immobilized with silver nanoparticles. *J. Mol. Struct.* **2021**, *1239*, 130496.
https://doi.org/10.1016/j.molstruc.2021.130496.

13. Khan, M. D.; Singh, A.; Khan, M. Z.; Tabraiz, S.; Sheikh, J. Current perspectives, recent advancements, and efficiencies of various dye-containing wastewater treatment technologies. *J. Water Proc.engineering* **2023**, *53*, 103579.
https://doi.org/10.1016/j.jwpe.2023.103579.

14. Klimenkov, O. M.; Ivanenko, I. M.; Hutsul, K. R.; Shust, V. I. Sol-Gel Synthesis OF ZnO Photocatalyst For Diclofenac Degradation. *Environ. Saf. Technol. Environ. Prot.* **2023**, *5*, 64–70.

15. Liang, X.; Hou, W.; Xu, Y.; Sun, G.; Wang, L.; Sun, Y.; Qin, X. Sorption of lead ion by layered double hydroxide intercalated with diethylenetriaminepentaacetic acid. *Colloids Surf. Physicochem. Eng. Aspects* **2010**, *366* (1), 50–57. https://doi.org/10.1016/j.colsurfa.2010.05.012.

16. Lacerda, E. H. C.; Lacerda, L. H. d. S.; Andrade, A. V. C. d.; Fujiwara, S. T.; Kloss, J. R. Spectroscopic, mineralogical and photocatalytic characterization of bentonite clay: A jointed DFT and experimental approach. *J. Photochem. Photobiol. A: Chem.* **2023**, *445*, 115077.
https://doi.org/10.1016/j.jphotochem.2023.115077.

17. Murakami, N.; Ono, A.; Nakamura, M.; Tsubota, T.; Ohno, T. Development of a visible-light-responsive rutile rod by site-selective modification of iron(III) ion on {1 1 1} exposed crystal faces. *Appl Catal B-Environ* **2010**, *97*, 115–119. https://doi.org/10.1016/j.apcatb.2010.03.030.

18. Philips-Invernizzi, B.; Dupont, D.; Caze, C. Bibliographical review for reflectance of diffusing media. *Opt. Eng.* **2001**, *40*, 1082–1092. https://doi.org/10.1117/1.1370387.

19. Pourhakkak, P.; Taghizadeh, M.; Taghizadeh, A.; Ghaedi, M. Chapter 2 - Adsorbent. In *Interface Sci*, Ghaedi, M. Ed.; Vol. 33; Elsevier, 2021; pp 71–210.

20. Olivera, S.; Nataraj, D.; S Puthran, A.; Dinesh, A.; Venkatesh, K.; Muralidhara, H. Alpha-Cellulose Derived from Teakwood Sawdust for Cationic Dyes Removal. *Mater. Focus* **2018**, *7*. https://doi.org/10.1166/mat.2018.1490.

21. Zhang, W.; Hu, Y.; Ma, L.; Zhu, G.; Wang, Y.; Xue, X.; Chen, R.; Yang, S.; Jin, Z. Progress and Perspective of Electrocatalytic CO_2 Reduction for Renewable Carbonaceous Fuels and Chemicals. *Adv. Sci.* **2018**, *5* (1), 1700275.
https://doi.org/10.1002/advs.201700275.

22. Zhuang, Y.; Yu, F.; Ma, J.; Chen, J. Facile synthesis of three-dimensional graphene–soy protein aerogel composites for tetracycline adsorption. *Desalination and Water Treat*. **2016**, *57* (20), 9510–9519. https://doi.org/10.1080/19443994.2015.1029530.

23. Zhuang, Y.; Zhang, H.; Ma, P.; Jiang, T.; Yang, Y.; Milliken, R.; Hsu, W. Visible and near-infrared reflectance spectra of igneous rocks and their powders. *Icar* **2022**, *391*, 115346. https://doi.org/10.1016/j.icarus.2022.115346.

АДСОРБЦІЙНІ ТА ФОТОКАТАЛІТИЧНІ ВЛАСТИВОСТІ ГЕТЕРОПЕРЕХОДУ ZnO/БЕНТОНІТ/Ag

Кліменков О.М.[1], Іваненко І.М.[1]

[1]Національний технічний університет України

«Київський політехнічний інститут імені Ігоря Сікорського», Україна

aleshaklemenkov@gmail.com

Деструкція органічних забрудників стічних вод різного походження є важливим науковим завданням, особливо на тлі сьогоднішніх реалій росту попиту на барвники в різних галузях промисловості. Перспективним рішенням цього завдання є розробка ефективних та екологічних способів деструкції органічних полютантів до простих та нетоксичних сполук за допомогою новітніх фотокаталізаторів. Синтез проводився новітнім методом золь-гель, проводились дослідження структурно-кристалічних, фазових та елементних параметрів за допомогою рентгенофазового аналізу, хімії поверхні використовуючи інфрачервону спектроскопію, розраховували ширину забороненої зони на основі спектроскопії дифузійного відбиття, адсорбційної та фотокаталітичної активності напівпровідникового фотокаталізатора ZnO та його гетеропереходів на основі бентоніту за допомогою УФ-спектроскопії. Синтезовані фотокаталізатори були використані для видалення барвника малахітового зеленого. Дослідження рівноваги для адсорбції проводилися з використанням ізотерм Ленгмюра та Фрейндліха, і кращої відповідності було досягнуто з моделлю Ленгмюра. Максимальна адсорбційна здатність була розрахована як 70,4 мг/г за допомогою рівняння Ленгмюра. Кінетичні параметри показали, що адсорбція малахітового зеленого на бентоніті відповідає моделі кінетики першого порядку, де k_1=0,152 хв$^{-1}$. Досліджувалась ефективність фотодеградації ZnO, ZnO/бентоніт та Zn/бентоніт/Ag у статичному експерименті під ультрафіолетовим опроміненням. За 60 хвилин вдалося досягти 99,4% фотодеградації розчину малахітового зеленого концентрацією 100 мг/дм^3 за допомогою потрійного гетероперехідного фотокаталізатора. Протягом лише 10 хвилин у присутності потрійного композиту вдалося досягти ступеня фотокаталітичної деградації на рівні 72%, що значно перевершує результати подвійного гетероперехідного фотокаталізатора. Отже, синтезований гетероперехід демонструє високу фотокаталітичну активність, яка значно виявляється впродовж коротких часових інтервалів. Запропоновано механізм фотокаталітичної деградації малахітового зеленого на основі літературних джерел.

Ключові слова: *бентоніт, гетероперехід, золь-гель, малахітовий зелений, фотокаталізатор, цинк оксид*